Engineering Structures 232 (2021) 111831

Contents lists available at ScienceDirect

Engineering Structures

journal homepage: www.elsevier.com/locate/engstruct

Fatigue performance evaluation for composite OSD using UHPC under dynamic vehicle loading

Lu Deng [a,b], Shengquan Zou [b], Wei Wang [a,b,*], Xuan Kong [a,b]

[a] Key Laboratory of Damage Diagnosis for Engineering Structures of Hunan Province, Hunan Univ., Changsha, China
[b] College of Civil Engineering, Hunan Univ., Changsha, China

ARTICLE INFO

Keywords:
Ultra-high performance concrete (UHPC)
orthotropic steel deck (OSD)
Composite bridge deck
Fatigue reliability evaluation
Dynamic vehicle loading

ABSTRACT

A novel composite orthotropic steel deck (OSD) using ultra-high performance concrete (UHPC) is comprised of an OSD and a thin UHPC layer that are connected through shear connectors. The innovative composite OSD system has been increasingly applied to long-span bridges in China to overcome the defect of conventional OSD that frequently suffers from fatigue cracking. However, the fatigue performance of the composite OSD system is usually evaluated with the deterministic analysis in previous studies, which may lead to inaccurate evaluation as many uncertainties, including the statistical properties of dynamic vehicle loadings and fatigue-prone details, have not been considered rationally. In this paper, the fatigue performance of the composite OSD using UHPC was investigated using the reliability-based fatigue analysis and compared with the fatigue performance of conventional OSD system. A three-dimensional vehicle-bridge coupled system was adopted to obtain the stress time histories of fatigue-prone details in the bridge decks under the action of dynamic vehicle loading. The vehicle model was determined based on the fatigue load pattern adopted in the AASHTO standard specifications and finite element models (FEMs) of both the conventional OSD and the composite OSD using UHPC were built based on a girder segment adopted from the HuMen Bridge in China. Four key influence factors, namely, the road surface condition (RSC), length of bridge deck FEM, vehicle speed, and overloading, were taken into consideration. The fatigue life of six typical fatigue-prone details in these two deck systems was evaluated and compared. The results show that the composite OSD using UHPC can effectively extend the fatigue life of OSD by at least 60% and even eliminate the risk of fatigue cracking for most fatigue-prone details. Compared to the reliability method, the fatigue life of OSD determined based on the deterministic method would be overestimated by 65–110% if the very poor RSC is considered. Besides, the composite OSD using UHPC exhibits a better fatigue performance than the conventional OSD system under the action of overloaded trucks. The results from the study can provide a reference for the design and maintenance of the composite OSD using UHPC.

1. Introduction

The conventional orthotropic steel deck (OSD), which is generally constituted by an OSD overlaid with an asphalt concrete pavement and is supported by longitudinal stiffeners and transverse beams, has been widely used in the long-span bridge around the world due to its advantages of life-cycle economy, high weight-to-strength ratio, and easy construction [1,2]. However, many studies have indicated that the conventional OSD system has frequently suffered from premature fatigue cracking under the action of cyclic traffic loadings [3–5]. Although many attempts have been made to improve the fatigue performance of OSD [6,7], the long-term effect of those improvements is still not satisfying. Based on the core concept of evenly distributing the local tire force and reducing the local stress of steel bridge deck, an innovative composite OSD using ultra-high performance concrete (UHPC) was proposed and has been increasingly applied to the rehabilitation of old bridges as well as the newly-built long-span bridge in China [8]. In such a system, a thin UHPC layer is cast on the OSD and short-headed studs are adopted as shear connectors.

Plenty of researches on the basic performance of the composite OSD using UHPC have been conducted. Abdelbaset et al. [9] found that the countermeasure employing UHPC layer on the OSD can significantly improve the stiffness of bridge deck, thus effectively reducing the hot stress of welded connections. Yuan et al. [10] verified the efficiency of

* Corresponding author at: Key Laboratory of Damage Diagnosis for Engineering Structures of Hunan Province, Hunan Univ., Changsha, China.
E-mail address: wang_wei@hnu.edu.cn (W. Wang).

https://doi.org/10.1016/j.engstruct.2020.111831
Received 15 May 2020; Received in revised form 1 December 2020; Accepted 28 December 2020
Available online 24 January 2021

UHPC overlay in improving the fatigue performance of OSD by comparing the fatigue behavior of OSD without pavement and casting UHPC as overlay under the same load condition. Ding and Shao [11] indicated that the stresses induced by vehicles are significantly reduced in the composite OSD using UHPC. Shao and Cao [12] further found that the risk of the innovative composite OSD suffering from fatigue cracking can be greatly reduced or even be effectively eliminated, which was also confirmed by Zhang et al. [13] based on the finite element analysis and fatigue tests. Liu et al. [14] revealed the influence of mechanical degradation of studs and the UHPC on the transverse fatigue performance of the composite OSD using UHPC. Besides, Zhu et al. [15] analyzed and predicted the fatigue lives of several fatigue-prone details in the composite OSD using UHPC based on the field monitoring data and the finite element analysis. However, in these previous studies, parameters used for the fatigue performance evaluation of the composite OSD using UHPC, including the dynamic vehicle loading and related parameters of fatigue-prone details, were regarded as deterministic variables, which may result in overestimation of the fatigue performance [16]. Therefore, there is a pressing need to reevaluate the fatigue performance of the composite OSD using UHPC from a reliability perspective. In addition, overloaded trucks can induce larger stress ranges which will accelerate the accumulation of fatigue damage. Therefore, the impact of overloading on fatigue performance of the composite OSD system also needs to be investigated. Besides, it should be noted that drawbacks of *S-N* curve and Miner's rules were not considered in this paper, such as the overload cycles may increase the fatigue life of components in certain cases [17,18].

In this paper, a three-dimensional vehicle-bridge coupled system was established and used for obtaining the stress time histories of six typical fatigue-prone details. The analytical model of vehicle was determined based on the fatigue load pattern adopted in the AASHTO standard specifications [19] and the finite element models (FEMs) of both the composite OSD using UHPC and the conventional OSD were built based on a local girder segment adopted from the HuMen Bridge in China. The influences of four key factors, namely, the road surface condition (RSC), length of bridge deck FEM, vehicle speed and vehicle overloading, on the stress range of the fatigue-prone detail and thus on the fatigue performances of the composite OSD using UHPC and the conventional OSD were investigated. Fatigue lives of those two OSD systems were evaluated and compared based on the fatigue reliability analysis. Besides, the rationality of the deterministic method for the fatigue limit state analysis adopted in the AASHTO standard specifications [19] was also discussed. The paper aims to evaluate the fatigue performance of the composite OSD using UHPC from a perspective of reliability and provide references for the design and maintenance of the composite OSD using UHPC.

2. Model of bridge deck

In this paper, FEMs of bridge decks were established based on a local girder segment of the HuMen Bridge, which is a suspension bridge with bidirectional six lanes and a main span of 888 m in China. Its original bridge deck was designed as a conventional OSD system, in which a 70-mm-thick asphalt pavement was overlaid on the OSD. The bridge deck was later modified into a novel composite OSD system to improve the fatigue performance, in which a thin UHPC layer with a thick of 45 mm was first cast on the OSD and an asphalt wearing course with a thick of 20 mm was then concreted on the UHPC layer. The short-headed studs with a height of 35 mm were used as shear connectors to strength the connection between the OSD and the UHPC layer. Structural details of the composite OSD using UHPC and the conventional OSD are shown in Fig. 1, and six typical fatigue-prone details (i.e., Detail 1–6) in the OSD [5] to be investigated are illustrated in Fig. 2.

The stress response of structural members in the OSD is mainly affected by the local load applied to the bridge and the affected area of the local load is fairly limited [20]. Therefore, there is no need to build the global FEM for a large-scale bridge when only the local area of interest is considered [21]. In the present study, a local girder segment of the middle lane in the HuMen Bridge was selected for analysis. The local FEM of bridge decks was established with the ANSYS 18.0 program based on the design scheme. As an example, the local FEM of the composite OSD using UHPC is illustrated in Fig. 3, which is supported by eight ribs and four diaphragms.

In these FEMs, the steel plates were modeled using the shell element SHELL91 with eight nodes, and the UHPC layer as well as the asphalt overlay were modeled using the solid element SOLID95 with twenty

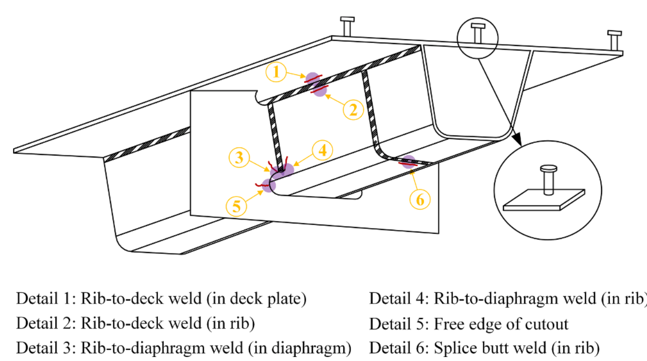

Fig. 2. Location of typical fatigue-prone details and corresponding fatigue cracks.

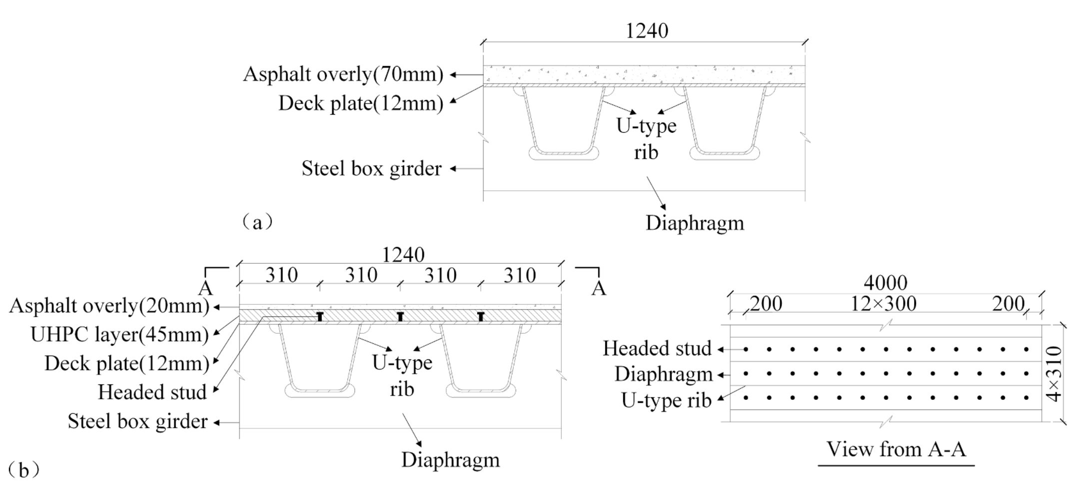

Fig. 1. Structural details of the bridge decks (mm): (a) the conventional OSD; (b) the composite OSD using UHPC.

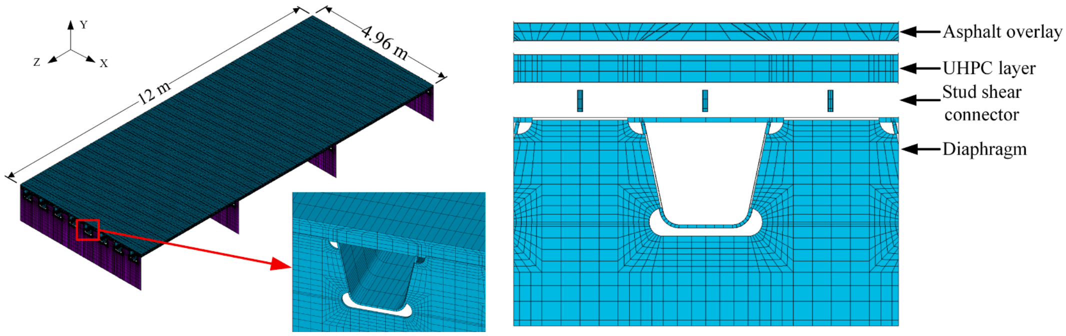

Fig. 3. Local FEM of the composite OSD using UHPC.

nodes. The studs were simulated using the beam element BEAM189 [11]. The mechanical properties of these materials were listed in Table 1. It should be noted that the nonlinearity of these materials were not considered in the study as previous studies have confirmed that the maximum stresses and strains in the steel plate and UHPC are far below the ultimate strength and can meet the design requirement [8,15]. Besides, the International Institute of Welding [22] requires that the mesh size of elements near hot spots shall be refined enough to obtain accurate hot spot stresses. In fact, for the FEM employing higher-order elements (e.g. eight-node shell elements), it is reasonable to use the mesh size of $t \times t$ near the hot spot, where t is the deck thickness at weld toe [23]. Considering that the thickness of steel plates connected by the weld joint is different, the minimum mesh size of elements was selected as 0.5 t at the area near fatigue-prone details. The mesh size gradually increased with the increase of distance far away from the considered area and was set as consistent with the extrapolation method, as listed in Table 4.

According to the Saint Venant principle, stress responses of the target areas far away from boundaries in the OSD are hardly affected by the boundary conditions, which has been confirmed by other researchers [24]. To simulate the actual boundary conditions as accurately as possible, the Z-axis translational degree of freedom (DOF) as well as the X- and Y-axis rotational DOF of nodes at both ends of the bridge deck were constrained, except for that of the end-diaphragms. The X-axis translational DOF as well as the Y- and Z-axis rotational DOF of nodes at either side of the deck and diaphragms were constrained to simulate the action applied by the adjacent steel box girders. The Y-axis translational DOF of nodes at the bottom of diaphragms were constrained to model the vertical support of diaphragms. In these FEMs, the following strategies are used to model the interaction between adjacent components. The nodes at the bottom of the asphalt layer were coupled to the nodes with the same coordinates at the top of the UHPC layer. Assuming that the short-headed studs will not separate from the UHPC layer under the action of vehicle loading and considering that the bottoms of short-headed studs are welded to the steel deck plate, the upper nodes of short-headed studs were coupled with the nodes of the UHPC layer with the same coordinates, and the nodes at the bottom of the short-headed studs were coupled to the corresponding nodes of the steel deck plate. For the nodes at the bottom of the UHPC layer, only the vertical translation was coupled to the corresponding nodes of the steel deck plate so that the UHPC layer will not separate from the steel deck plate while the shear and friction action of the interface between them were ignored [25].

Table 1
Mechanical properties of the model material.

Material	Young's modulus (GPa)	Poisson's ratio	Density (kg/m^3)
Steel	210	0.3	7850
UHPC	42.6	0.2	2700
Asphalt	2	0.2	2400

3. Model of fatigue truck

The model of fatigue truck, as shown in Fig. 4, was modified from a typical 5-axis truck model (Type 9) that was presented by Wang and Liu [26] based on the survey data of trucks in the United States. Using the force and the moment equilibrium equations, the geometry, mass distribution, and inertia moment of the fatigue truck were determined based on the load pattern for the fatigue design of OSDs adopted in the AASHTO standard specifications [19]. Table 2 summarizes the detailed parameters of the fatigue truck.

4. Vehicle-Bridge coupled system

A three-dimensional vehicle-bridge coupled system proposed by Deng and Cai [27] was used to obtain vehicle-induced responses of the composite OSD using UHPC and the conventional OSD in this paper. The coupled equation can be expressed as follows:

$$\begin{bmatrix} M_d & M_v \end{bmatrix} \begin{Bmatrix} \ddot{d}_d \\ \ddot{d}_v \end{Bmatrix} + \begin{bmatrix} C_d + C_{d-d} & C_{d-v} \\ C_{v-d} & C_v \end{bmatrix} \begin{Bmatrix} \dot{d}_d \\ \dot{d}_v \end{Bmatrix} + \begin{bmatrix} K_d + K_{d-d} & K_{d-v} \\ K_{v-d} & K_v \end{bmatrix} \begin{Bmatrix} d_d \\ d_v \end{Bmatrix} = \begin{Bmatrix} F_d \\ F_v + F_G \end{Bmatrix} \tag{1}$$

where the subscripts (i.e., d and v) mean the bridge deck and the vehicle, respectively; M_d, M_v, C_d, C_v, K_d, and K_v represent the matrixes of mass, damping and stiffness, respectively; $C_{d\text{-}d}$, $C_{d\text{-}v}$, and $C_{v\text{-}d}$ represent the damping relevant terms, and $K_{d\text{-}d}$, $K_{d\text{-}v}$, and $K_{v\text{-}d}$ represent the stiffness relevant terms, all of which are induced by the interaction between the pavement and wheels; d_d and d_v represent the vectors of displacement; F_d and F_v represent the vectors of wheel-pavement interaction force; and F_G represents the vector of vehicle weight acting on the bridge.

Since it is very time-consuming to solve Eq. (1) directly, the mode superposition technology can be used to reduce the matrix size, as indicated in the other work of the first author [28]. Once Eq. (1) is solved, the stress time histories of fatigue-prone details can be obtained according to the strain–displacement relationship and the stress–strain relationship. It should be noted that the accuracy and reliability of the adopted bridge-vehicle model has been verified in other works of the first author through field tests on a field bridge in Louisiana [29,30], in which the bridge responses, including deflections and strains at the mid-span of the girders, were measured and compared with the bridge responses obtained from the numerical simulations. The field measured results and the numerical results agree with each other very well, in terms of both maximum dynamic responses and the vibration frequencies.

5. Deterioration model of RSC

The RSC is one of the main factors affecting the interaction between

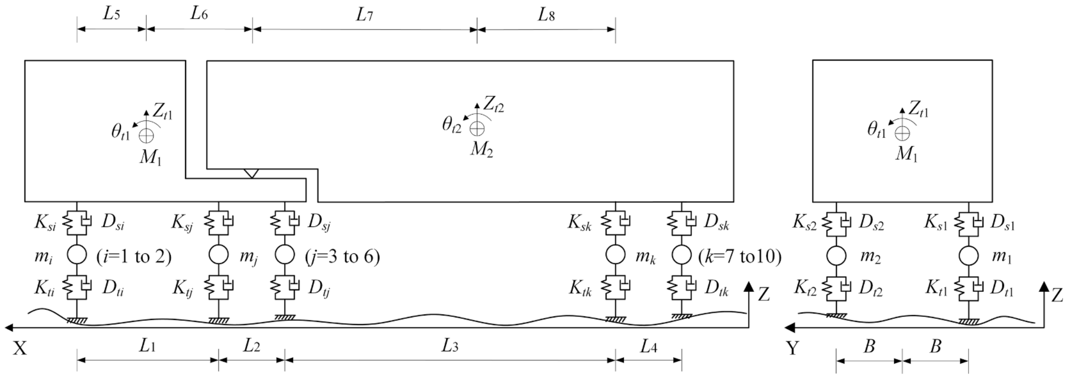

Fig. 4. Analytical model of the fatigue truck.

Table 2
Detailed parameters of the fatigue truck.

Items	Parameters	Values	Units
Mass	M_1	5045	kg
	M_2	23,070	kg
	m_i $(i = 1–2)$	297	kg
	m_j $(j = 3–6)$	466	kg
	m_k $(k = 7–10)$	527	kg
Moment of inertia	I_{XZ1}	17,595	Kg·m^2
	I_{XZ2}	270,157	kg·m^2
	I_{YZ1}	4399	kg·m^2
	I_{YZ2}	26,935	kg·m^2
Spring stiffness	K_{si} $(i = 1–2)$	485,101	N/m
	K_{ti} $(i = 1–2)$	1,402,416	N/m
	K_{sj} $(j = 3–6)$	697,880	N/m
	K_{tj} $(j = 3–6)$	2,804,656	N/m
	K_{sk} $(k = 7–10)$	679,667	N/m
	K_{tk} $(k = 7–10)$	2,804,656	N/m
Damping coefficient	D_{si} $(i = 1–2)$	2399	N·s/m
	D_{ti} $(i = 1–2)$	1600	N·s/m
	D_{sj} $(j = 3–6)$	3606	N·s/m
	D_{tj} $(j = 3–6)$	1600	N·s/m
	D_{sk} $(k = 7–10)$	3786	N·s/m
	D_{tk} $(k = 7–10)$	1600	N·s/m
Length	L_1	3.658	m
	L_2	1.219	m
	L_3	7.925	m
	L_4	1.219	m
	L_5	1.698	m
	L_6	2.569	m
	L_7	4.922	m
	L_8	3.613	m
	B	0.914	m

the bridge and vehicle, which can significantly affect the vehicle-induced stress range [31]. A stationary Gaussian random process with zero mean was adopted to model the road surface roughness [32], which can be generally expressed as an inverse Fourier transformation:

$$r(Z) = \sum_{i=1}^{N} \sqrt{2\varphi(n_i)\Delta n} cos(2\pi n_i Z + \theta_i) \tag{2}$$

where Z is the longitudinal position of interest points; $\varphi()$ is a function describing the road surface profile, which is adopted as the power spectral density function presented by Huang et al. [33,34]; θ_i is the phase angle which is randomly generated and uniformly distributed in the range from 0 to 2π; and n_i is the number of waves.

Based on the road roughness classification index defined by the ISO [35] and the road roughness classification of pavement calculated at time t during its service period, Zhang and Cai [16] presented a deterioration pattern of RSC during a 15-year service period, as described in Table 3.

Table 3
Deterioration pattern of RSC during a 15-year service period [16].

RSC classification	A (Very good)	B (Good)	C (Average)	D (Poor)	E (Very poor)
Time(t)/years	$1 \le t \le 8$	$9 \le t \le 10$	$11 \le t \le 12$	$t = 13$	$14 \le t \le 15$
Percentage	53.3%	13.3%	13.3%	6.7%	13.3%

Table 4
Stress analysis method for each fatigue-prone detail.

Detail	Analysis method	Type of hot spot	Extrapolation formula*	Stress type	Source
1	Hot spot stress	c	$\sigma_{hot} = 1.5\sigma_{0.5t} - \sigma_{1.5t}$	*SX*	[22]
2	Hot spot stress	c	$\sigma_{hot} = 1.5\sigma_{0.5t} - \sigma_{1.5t}$	*SY'/* **SY''**	[22]
3	Hot spot stress	b	$\sigma_{hot} = 1.12\sigma_5$	*S1*	[51]
4	Hot spot stress	a	$\sigma_{hot} = 1.5\sigma_{0.5t} - \sigma_{1.5t}$	*SZ*	[22]
5	Nominal stress	——	——	*S1*	——
6	Nominal stress	——	——	*SZ*	——

Note: (a) t = the deck thickness at weld toe; $\sigma_{0.5t}$, $\sigma_{1.5t}$, and σ_5 = the stresses at reference points 0.5 t, 1.5 t, and 5 mm away from the weld toe, respectively; (b) the coordinate direction was shown in Fig. 5.

6. Numerical analysis

The important factors affecting the interaction between the bridge and vehicle have been widely investigated [16,33]. Based on those researches, the influences of three key parameters, namely, the RSC, length of bridge deck FEM and vehicle speed, on the stress time histories experienced by the fatigue-prone details under consideration were investigated using the vehicle-bridge coupled system in this section. Five different RSCs listed in Table 3, three different lengths of the bridge deck FEM (i.e., 12 m, 16 m, and 20 m) as well as six vehicle speeds (i.e., 20 km/h, 40 km/h, 60 km/h, 80 km/h, 100 km/h, and 120 km/h) were considered. Based on previous studies [15,36], the most unfavorable stress range of fatigue details may occur when the vehicle travels across the bridge along these three critical travelling paths shown in Fig. 5. Therefore, these three critical travelling paths were adopted in the study.

Compared to the nominal stress method, the another commonly-used approach to obtaining the local stress of interest, namely the hot-spot stress method, achieves a higher accuracy and requires less efforts to deal with the FEM of welded connections in the complex structures [37].

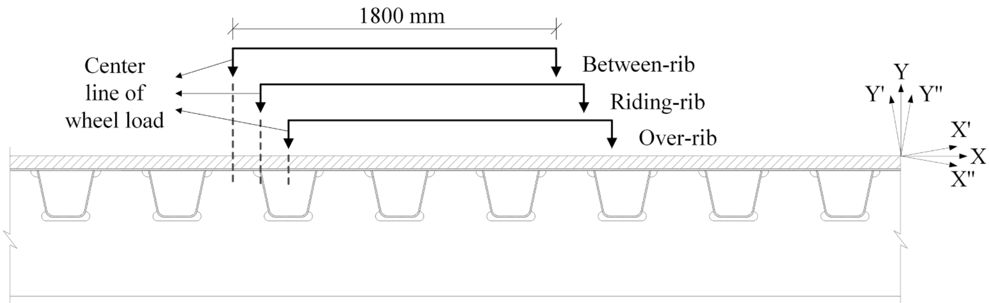

Fig. 5. Illustration of typical transverse loading cases.

In fact, hot spots are the crack initiation points of weld toes where weld defects may exist [22], as shown in Fig. 6(a). Since the steel plate around the fatigue-prone details was meshed to be consistent with the corresponding extrapolation path, the hot-spot stresses of concerned details can be determined based on the stress-extrapolation method (as described in Fig. 6(b)) once the stresses of reference points are obtained by the previously described vehicle-bridge coupled system. Considering that Details 1–4 are welded details, Detail 5 is a cutout detail with a smooth cut and Detail 6 is a continuous detail [13], the extrapolation method was chosen to obtain the stress of each fatigue-prone detail in this study, as listed in Table 4. It should be noted that the effect of residual tensile stress on the fatigue performance of fatigue details is not analyzed specifically in this paper since it is usually considered in the experiments to obtain *S-N* curves [38].

In addition, the road surface profile was generated based on a random process, which will result in bias for the simulation results. Therefore, the vehicle-bridge coupled system was repeatedly carried out 20 times for each case with a given RSC, and the average value of 20 simulated results was obtained for analysis, which has been confirmed to be acceptable [39].

6.1. Revised equivalent stress range

As the bridge deck system would be subjected to complex stress cycles when trucks travel across the bridge, the fatigue damage of bridge members accumulates with the increase of service time. In this paper, accumulated fatigue damage at time t was calculated as [40]:

$$D_t = \sum_i \frac{n_i}{N_i} \tag{3}$$

where n_i is the number of stress cycle corresponding to the ith constant-amplitude stress range (S_i) induced by the vehicle; N_i is the total number of S_i as fatigue failure occurs, and can be expressed as [41]:

$$N_i = \frac{K}{S_i^m} \tag{4}$$

where K is the fatigue strength coefficient related to the detail category; m is the slope of S–N curve, taken as 3 for all fatigue-prone details in the study [19].

It can be observed from Eqs. (3) and (4) that the accumulated fatigue damage (D_t) is affected by the number and the magnitude of stress range. Therefore, a revised equivalent stress range (RESR) was defined in this study to facilitate the calculation and analysis of fatigue damage accumulation induced by per truck, as expressed in Eq. (5):

$$\mathrm{RESR} = \left(\sum_i n_i S_i^m\right)^{1/m} \tag{5}$$

It should be noted that n_i and S_i in Eq. (5) were calculated by rainflow counting method, and any S_i less than the cutoff value, namely 3.45 MPa [42], was ignored. Coalescing Eqs. (3)–(5), the accumulated fatigue damage can be expressed as:

$$D_t = \frac{\mathrm{RESR}^m}{K} \tag{6}$$

6.2. Effects of bridge model length and RSC on RESR

The study on simple-supported steel girder bridges shows that the span length has significantly effects on the number of stress cycles under traffic loads when the bridge span is shorter than 22.86 m [43]. In addition, the length of the adopted fatigue truck is about 14 m that is close to the length of the bridge deck FEM in Fig. 3. Therefore, it is necessary to determine a reasonable length for the bridge model such that a good balance can be achieved between the computing efficiency and accuracy. In the study, FEMs of the bridge deck with different lengths (i.e., 12 m, 16 m, and 20 m), were established. Assuming the speed of fatigue truck is 60 km/h, the RESRs of the considered details under different RSCs were obtained. The most unfavorable RESRs of each fatigue-prone detail against different lengths of bridge models are illustrated in Fig. 7. Smooth, namely the case without considering the effect of RSC, is also included in Fig. 7 for comparison.

As shown in Fig. 7, the most unfavorable RESR of each fatigue-prone detail in both the composite OSD using UHPC and the conventional OSD

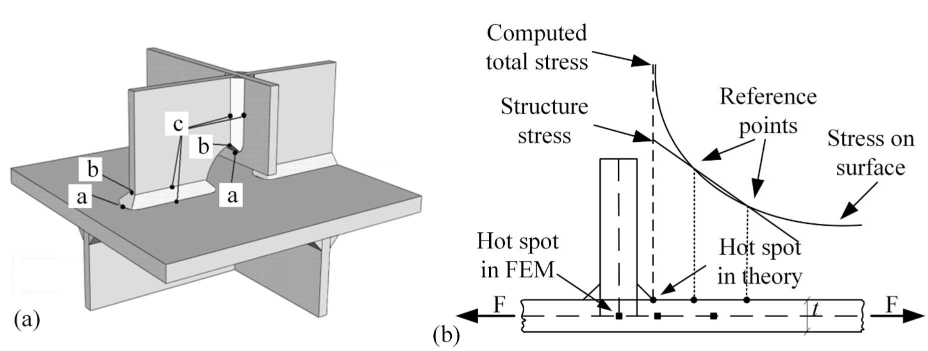

Fig. 6. Hot-spot stress method: (a) types of hot-spot; (b) stress-extrapolation method.

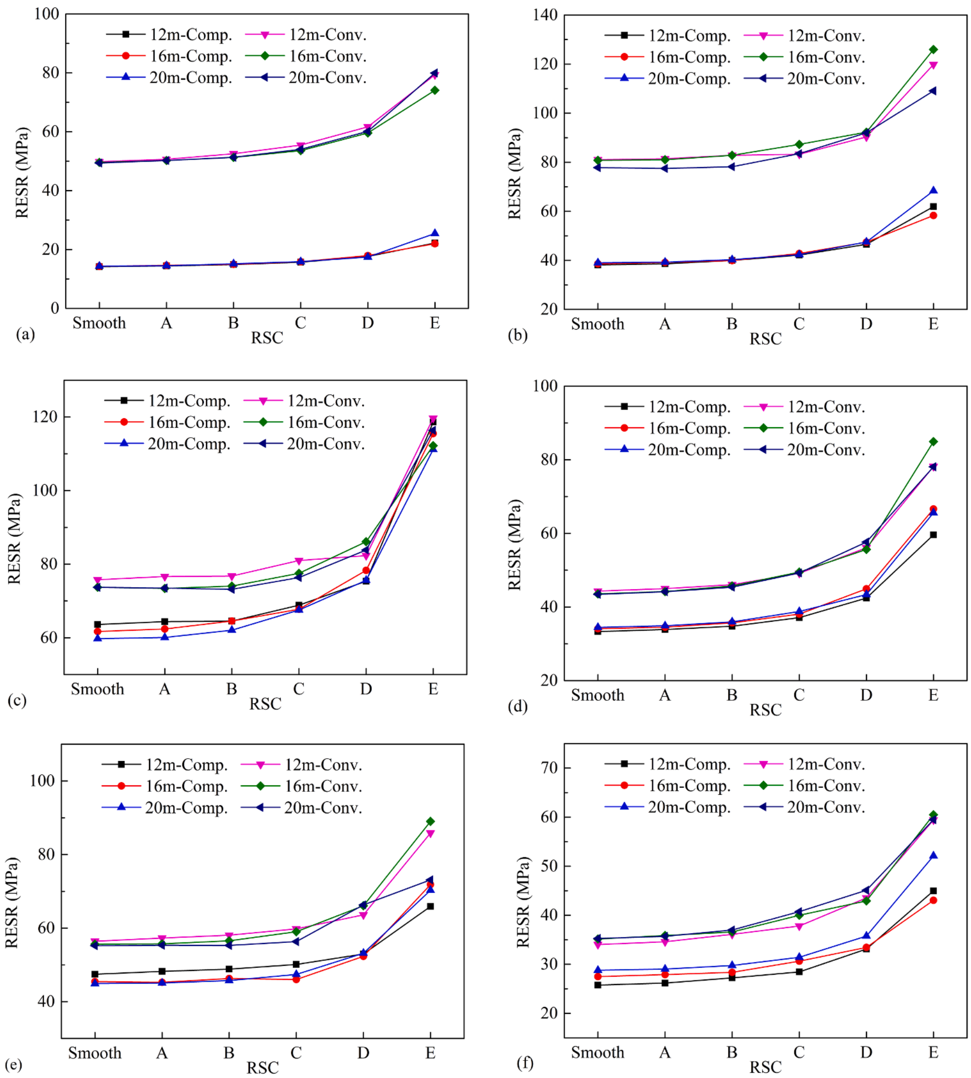

Fig. 7. Change of the RESR with length of the bridge deck FEM and RSC: (a) Detail 1; (b) Detail 2; (c) Detail 3; (d) Detail 4; (e) Detail 5; (f) Detail 6 (Note: Comp. = composite OSD using UHPC; Conv. = conventional OSD.)

is slightly influenced by the length of the bridge deck under different RSCs. As a matter of fact, it has been found that the vehicle-induced stress response of structural components in OSD can be observed only when the wheel load approaches the component [44], and the distance affected by wheel loads along the longitudinal direction is less than 3 m [36]. In other words, the boundary conditions of these fatigue-prone details in these FEMs with different lengths are remarkably similar. Therefore, it can be believed that the FEM adopting a length of 12 m is sufficient to balance the computing efficiency and accuracy effectively. Fig. 7 also shows that the RSC can significantly affect the RESRs of all fatigue-prone details in those two OSD systems. The RESR of Detail 3 in the conventional OSD under the very poor RSC is even more than 1.86 times of those under the very good RSC and the case of Smooth. Besides, it can be seen from Fig. 7 that the composite OSD using UHPC is effective to reduce the RESR of all fatigue-prone details in the OSD, especially for Detail 1 and Detail 2 whose RESR are decreased by more than 70% and 50%, respectively, compared to those in the conventional OSD.

6.3. *Effects of vehicle speed and RSC on RESR*

Many researches have indicated that there is no consistent conclusion about how the vehicle speed affects the vehicle-bridge interaction [39,45]. In order to investigate the influence of vehicle speed on the RESR and thus the accumulated fatigue damage of the composite OSD using UHPC, RESRs of the fatigue-prone details under different vehicle speeds and RSCs were obtained and plotted in Fig. 8.

As shown in Fig. 8, the variation pattern of RESR with the increase of vehicle speed under each RSC is not consistent. For all fatigue-prone details, the influences of vehicle speed on the RESR are not significant when the RSC ranges from class A to class D, while the RESR changes significantly and irregularly as the vehicle speed increases if the RSC becomes very poor (class E). This phenomenon was also observed from the studies about the conventional OSD [24] and beam bridges [46]. However, there has not been a convincing and consistent explanation for this phenomenon due to the complication of vehicle-bridge interaction caused by various factors simultaneously [47]. Besides, the vehicle speed corresponding to the maximum RESR is different under different RSCs due to the fact that increasing the vehicle speed does not necessarily intensify the bridge-vehicle interaction. Considering that the traffic speed of trucks on the Humen Bridge is restricted to 60 km/h, and that the RESR under this speed is relatively larger, the speed of fatigue truck was set as 60 km/h in the following fatigue reliability analysis.

In this section, the fatigue performance of the composite OSD using UHPC and the conventional OSD was evaluated and compared based on the fatigue reliability method and the deterministic method. Besides, the effects of RSC and overloading on the fatigue reliability of those two

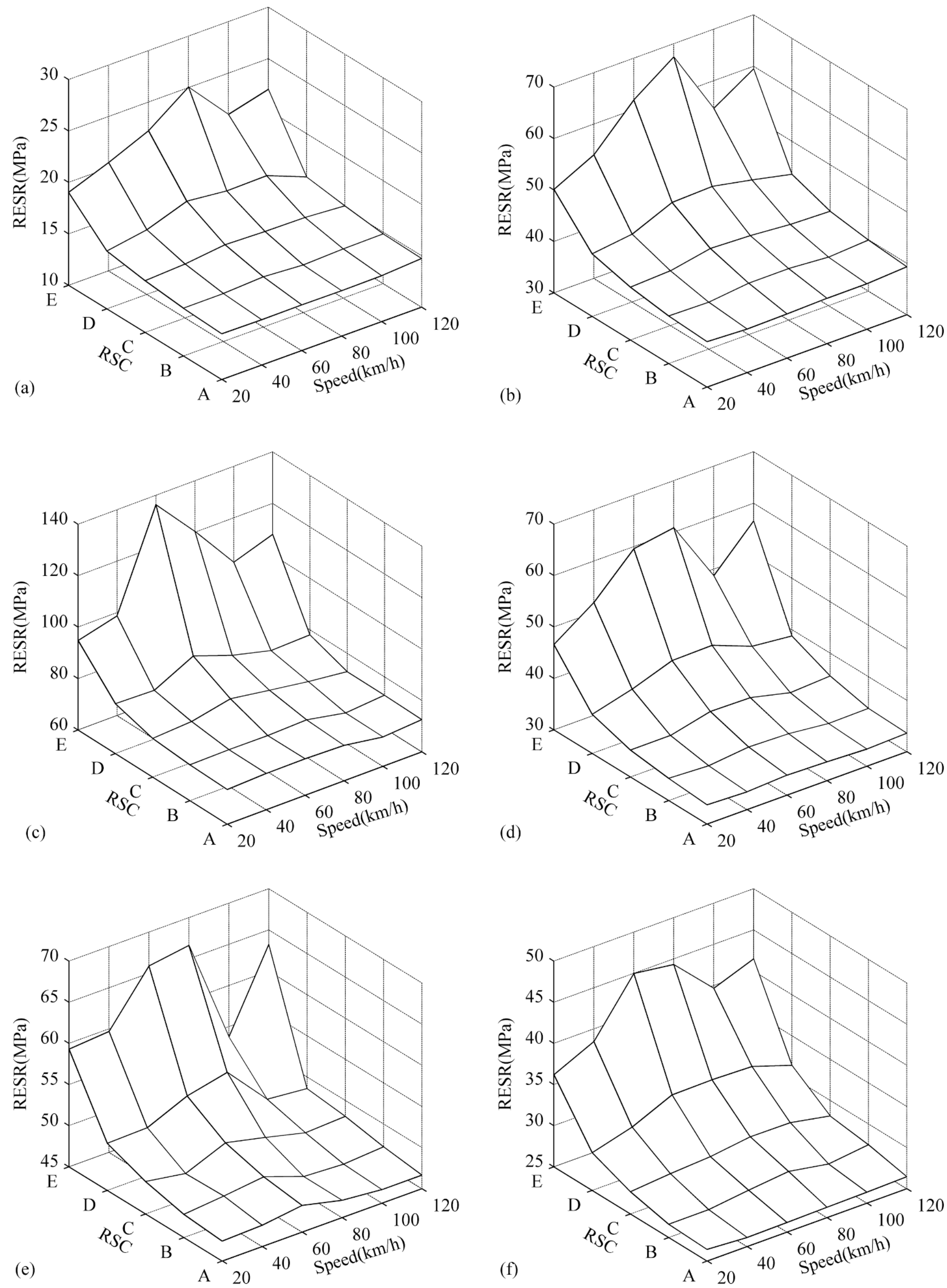

Fig. 8. Change of the RESR in the composite OSD with vehicle speed and RSC: (a) Detail 1; (b) Detail 2; (c) Detail 3; (d) Detail 4; (e) Detail 5; (f) Detail 6.

OSD systems were also investigated. In the analysis of fatigue reliability, the limit state function was expressed as:

$$g(X) = D_c - D_t \tag{7}$$

where D_c is the critical damage, and fatigue failure occurs when the failure function $g < 0$ [48].

Generally, the deterioration of pavement is a repetitive process and the proportion of time for each class of RSC staying in the lifecycle of bridge is approximately equal to that staying in a 15-year service period [46]. Therefore, the accumulated fatigue damages at time t can be calculated as a summation of the fatigue damages induced by all truck passages and can be expressed as follows:

$$D_t = \frac{N_t \sum_{j=1}^{5} a_j \left(\mathrm{RESR}_j\right)^m}{K} \tag{8}$$

where RESR_j is the RESR induced by a truck travelling across the bridge under the RSC of class j ($j = 1, 2, 3, 4$, and 5 corresponding to each class of RSC, namely A, B, C, D, and E, respectively); a_j is the proportion of time for RSC staying in the class j during the service time of bridge, as listed in Table 3; and N_t is the number of trucks travelling across the bridge for t years and can be calculated as:

$$N_t = 365 \cdot p \cdot \mathrm{ADTT} \cdot t \tag{9}$$

where p is the proportion of traffic in the lane considered and is taken as 0.85 in the study; ADTT is the average daily truck traffic in one direction, which is assumed to be 2000 in this study [19].

Coalescing Eqs. (7)–(9), the limit state function for reliability analysis of all fatigue-prone details can be re-expressed as:

$$g(X) = D_c - 365 \cdot p \cdot \mathrm{ADTT} \cdot t \cdot K^{-1} \sum_{j=1}^{5} a_j (\mathrm{RESR}_j)^m \tag{10}$$

Before calculating the fatigue reliability index of each fatigue-prone detail based on Eq. (10), it is essential to determine the statistical properties of each variable in Eq. (10). In order to obtain the distribution type of RESR using Chi-square test, the vehicle-bridge coupled system was performed 50 times under each case with a given RSC in this section. According to the Sturges' rule, the class number of a database with 50 samples was calculated as 7, and the degree of freedom should be set as 4 in the Chi-square test. Besides, the significance level was taken as 0.05 and the threshold value was determined to be 9.488. Two commonly-used distribution types, namely the normal distribution and the lognormal distribution, were considered in this study. The values of Chi-square test for the RESR of each fatigue-prone detail are listed in Table 5. Comparing the results of Chi-square test with the threshold value, it can be found that it is more acceptable to assume that the RESR follows the lognormal distribution in this study.

The statistical properties of RESRs under different RSCs are obtained and listed in Table 6, including the mean and the coefficient of variation (COV). Table 7 summarizes the statistical properties of other random variables for reliability analysis in Eq. (10) [42].

Using the iterative Rackwitz-Fiessler algorithm, the fatigue reliability indexes of fatigue-prone details in the bridge deck against the service time were calculated based on Eq. (10). Two conditions were considered in this study, as shown in Fig. 9, where Condition "a" took all five RSCs into account, and Condition "b" did not include the RSC of class E (very poor). In addition, the target reliability index (β_{target}) for bridge evaluation, which is taken as 2.5 in the AASHTO MBE code [49], is included in Fig. 9 for comparison.

As Fig. 9 shows, the fatigue reliabilities of all fatigue-prone details decline as the service time increases and the fatigue reliability index of each fatigue-prone detail in the composite OSD using UHPC is much greater than that in the conventional OSD under the same condition. Fig. 9 also shows that all fatigue-prone details in the composite OSD using UHPC can meet the requirement of the target reliability index over the design lifetime if the pavement maintenance could be carried out before the RSC deteriorates into the class of very poor, except for Detail 3 that may be caused by the defect in the initial design of the bridge deck [11]. By contrast, the fatigue reliability indexes of all fatigue-prone details except for Detail 5 in the conventional OSD will reduce to below the target reliability index after different service time. Specifically, it takes less than 15 years for the fatigue reliability indexes of Detail 2 and Detail 3 in the conventional OSD decreasing to the target reliability index. In addition, compared with that under Condition "b", the fatigue reliability index of all fatigue-prone details under Condition "a" is decreased by more than 1, which indicates that the vehicle dynamic effect can significantly affect the fatigue reliabilities of both the composite OSD using UHPC and the conventional OSD if the RSC deteriorates into the class of E (very poor).

The fatigue lives of fatigue-prone details in those two OSD systems evaluated with the reliability method and the deterministic method

Table 5
Values of Chi-square test for the RESR of each fatigue-prone detail.

Detail	RSC	Conventional OSD		Composite OSD	
		Normal	Lognormal	Normal	Lognormal
1	A	1.324	1.504	4.574	7.221
	B	5.635	6.310	2.413	0.573
	C	3.415	1.115	10.777	7.715
	D	10.104	4.552	2.443	3.136
	E	6.137	6.312	3.315	0.802
2	A	0.583	2.557	4.439	4.628
	B	3.432	2.376	2.692	0.704
	C	6.284	5.267	9.031	6.906
	D	2.551	5.515	0.690	2.913
	E	5.237	4.450	7.514	7.340
3	A	1.804	1.993	5.986	4.496
	B	11.806	5.929	4.005	4.628
	C	2.536	1.327	5.317	4.442
	D	6.545	6.281	1.712	6.517
	E	4.270	1.944	9.152	4.531
4	A	1.082	1.926	3.727	3.992
	B	2.627	2.073	2.926	2.915
	C	1.599	4.265	3.507	5.072
	D	2.064	1.642	5.311	0.851
	E	7.490	3.897	9.232	5.943
5	A	12.860	8.907	3.886	1.961
	B	6.569	4.097	7.322	2.453
	C	10.612	1.869	3.245	2.764
	D	12.934	5.391	1.270	3.681
	E	5.143	8.283	7.609	4.004
6	A	2.626	4.976	0.583	0.703
	B	4.582	7.809	1.358	3.202
	C	6.485	3.702	9.848	2.538
	D	10.733	4.888	1.632	2.141
	E	2.498	0.854	3.837	5.272

Table 6
Statistical properties of RESRs under different RSCs.

Detail	RSC	Conventional OSD		Composite OSD	
		Mean	COV	Mean	COV
1	A	50.65	0.0229	14.45	0.025
	B	52.28	0.0398	14.78	0.0408
	C	54.77	0.0799	15.51	0.0797
	D	60.78	0.1285	17.29	0.1283
	E	81.48	0.1977	22.92	0.2015
2	A	81.5	0.0287	38.63	0.022
	B	81.76	0.0607	39.83	0.0381
	C	82.86	0.0933	41.7	0.0788
	D	89.77	0.1721	45.87	0.124
	E	118.6	0.211	61.43	0.1932
3	A	75.67	0.0272	64.03	0.0242
	B	76.27	0.0586	64.84	0.0575
	C	79.61	0.0919	68.15	0.106
	D	85.61	0.1496	76.21	0.1143
	E	113.2	0.1944	111.5	0.1704
4	A	44.79	0.0189	33.75	0.0174
	B	45.92	0.0286	34.7	0.0284
	C	48.68	0.0528	36.8	0.051
	D	56.57	0.1007	42.73	0.1036
	E	79.54	0.1659	61.01	0.1634
5	A	56.74	0.0299	47.73	0.0301
	B	56.87	0.0592	47.86	0.0598
	C	58.76	0.084	49.21	0.0865
	D	65.12	0.1441	54.19	0.1532
	E	80.7	0.2381	65.61	0.2573
6	A	34.7	0.018	26.24	0.0156
	B	35.73	0.0399	27.13	0.0348
	C	37.71	0.0593	28.74	0.0598
	D	42.66	0.1209	32.48	0.1367
	E	59.72	0.1648	43.71	0.1701

Table 7
Statistical properties of random variables in the limit state function.

Parameter	Specification	Distribution type	Mean	COV	Source
D_c	Critical damage	Lognormal	1.0	0.3	[52]
K (Category A)	Detail 5	Lognormal	82.0×10^{12} (MPa^3)	0.45	[42]
K (Category C)	Detail 1–4	Lognormal	14.4×10^{12} (MPa^3)	0.45	[42]
K (Category D)	Detail 6	Lognormal	7.21×10^{12} (MPa^3)	0.45	[42]

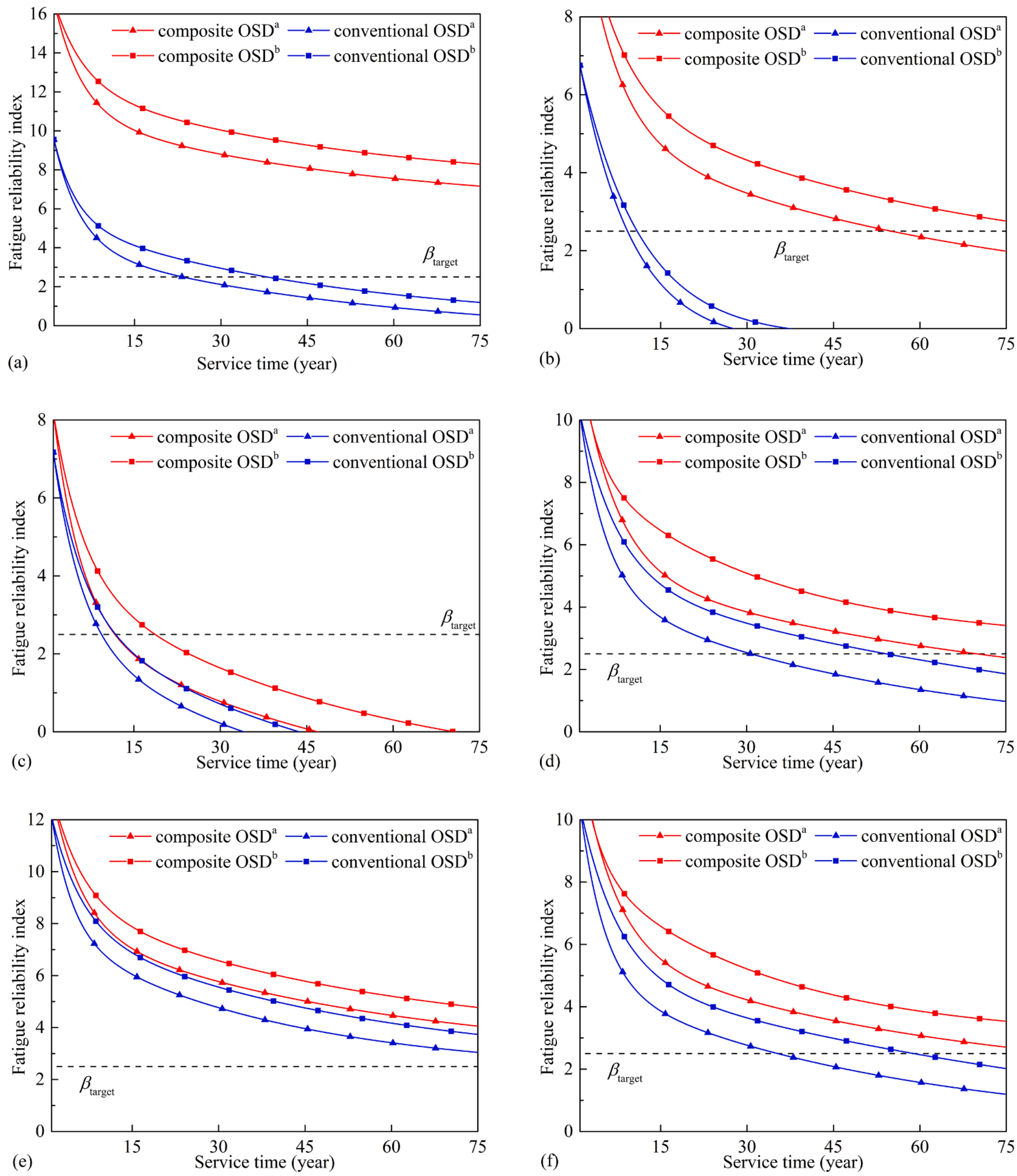

Fig. 9. Fatigue reliability indexes of fatigue-prone details against the service time: (a) Detail 1; (b) Detail 2; (c) Detail 3; (d) Detail 4; (e) Detail 5; (f) Detail 6.

were summarized in Table 8. The fatigue life of structural member evaluated with the reliability method was defined as the service time for its fatigue reliability index decreasing to the target reliability index (β_{target}) [50]. According to the AASHTO standard specifications [19], the fatigue life evaluated with the deterministic method was calculated as follows:

$$t = \frac{K}{365 \cdot p \cdot \text{ADTT} \cdot C_s \cdot [(1 + IM) \cdot \Delta S]^m} \tag{11}$$

where C_s is the number of stress cycles excited by each truck, taken as 5.0 for structural connections in the OSD; IM is the dynamic load allowance, taken as 0.15 for fatigue analysis [19]; and ΔS is the maximum static stress range.

Table 8 shows that the fatigue lives of fatigue-prone details in the composite OSD using UHPC are much larger than that in the conventional OSD. Particularly, the fatigue life of Detail 1 is expected to be more than 1000 years, which can be assumed to have an infinite fatigue life. Besides, the fatigue lives of all fatigue-prone details in those two OSD systems calculated based on Method 2 (deterministic method) are about 15–30% and 65–110% larger than that calculated based on the Method 1[b] and the Method 1[a], respectively, which indicates that the fatigue life obtained based on the deterministic method is overestimated

Table 8
Fatigue lives of fatigue-prone details using different methods (year).

Detail	Conventional OSD			Composite OSD		
	Method 1[a]	Method 1[b]	Method 2	Method 1[a]	Method 1[b]	Method 2
1	24	38	49	1039	1636	2133
2	7	10	12	55	86	104
3	8	12	14	11	19	23
4	31	54	62	70	125	146
5	113	159	189	190	269	317
6	35	58	72	85	133	161

Note: Method 1[a] and Method 1[b] represent the reliability method considering Condition “a” and Condition “b”, respectively; Method 2 represents the deterministic method.

significantly. The results in Table 8 also show that fatigue lives of fatigue-prone details in those two OSD systems under Condition "b" are 1.4–1.75 times longer under Condition "a", which indicates the significance of preventing the RSC from deteriorating to the class of very poor for prolonging the fatigue life of bridge decks.

Vehicle overloading is a progressively worse problem and the overloading ratio of trucks has been gradually growing. The weigh-in-motion data from a bridge nearby the HuMen Bridge shows the measured heaviest truck is even more than 160 t [15], which is several times heavier than the standard fatigue truck. Two typical overloading ratios (i.e., g = 20% and 50%) were considered to study the influence of vehicle overloading on the fatigue performance of the composite OSD using UHPC. The results are summarized in Table 9, including the fatigue lives of fatigue-prone details in the conventional OSD for comparison, where the values of fatigue life were evaluated using the reliability method under Condition "b", namely, Method 1^{b}.

It can be observed from Table 9 that the fatigue lives of both the composite OSD using UHPC and the conventional OSD are significantly affected by overloaded trucks. Specifically, fatigue lives of all fatigue-prone details are reduced by more than 35% when the truck weight increases by 20%, and the fatigue lives could be shortened by more than 60% if the overloading ratio reaches 50%. Compared to the conventional OSD, the composite OSD using UHPC can prolong the fatigue life of the bridge deck by at least 60% under the action of standard traffic load, and can prolong the fatigue life of the bridge deck by at least 80% when the overloading ratio reaches 50%. This indicates that the composite OSD system shows better fatigue performance than the conventional OSD system as the overloading ratio increases.

Table 9
Fatigue lives of fatigue-prone details under different overloading ratios (year).

Detail	Conventional OSD			Composite OSD		
	g = 0%	g = 20%	g = 50%	g = 0%	g = 20%	g = 50%
1	38	23	13	1636	1031	584
2	10	6	3	86	53	30
3	12	7	4	19	12	8
4	54	34	19	125	79	45
5	159	99	54	269	168	97
6	58	37	21	133	85	49

7. Conclusions

Based on the research results obtained from this study, the following conclusions and recommendations are drawn:

The fatigue life of bridge decks calculated based on the deterministic method is overestimated significantly. Specifically, fatigue lives of both the composite OSD using UHPC and the conventional OSD calculated based on the deterministic method are 65–110% longer than that calculated based on the reliability method if very poor RSC is considered.

The fatigue life of OSD is significantly affected by overloading. To be more specific, a 50% increment of the truck weight can reduce the fatigue life of the OSD by more than 60%. Nonetheless, the composite OSD using UHPC shows a better fatigue performance than the conventional OSD when subjected to overloaded trucks as the former contributes to the even distribution of tire load.

Compared to the conventional OSD, the composite OSD using UHPC can extend the fatigue life of OSD by at least 60% and the risk of suffering from fatigue cracking for most fatigue-prone details in the composite OSD using UHPC can be basically eliminated.

The RSC can significantly affect the fatigue reliabilities of both the composite OSD using UHPC and the conventional OSD. Particularly, their fatigue lives can be extended by 40–75% if pavement maintenance could be undertaken before the RSC deteriorates into the very poor condition.

It should be noted that the effect of corrosion on the fatigue evaluation was not considered in the study and that both the maintenance period of pavement and the deterioration pattern of RSC were hypothetically adopted from available literatures. It should also be noted that the effect of wind-induced bridge vibration on fatigue performance of the OSD system was not considered in the study.

CRediT authorship contribution statement

Lu Deng: Conceptualization, Methodology, Software, Supervision. **Shengquan Zou:** Software, Investigation, Data curation, Writing - original draft. **Wei Wang:** Validation, Investigation, Writing - original draft, Visualization. **Xuan Kong:** Writing - review & editing.

Declaration of Competing Interest

The authors declare that they have no known competing financial interests or personal relationships that could have appeared to influence the work reported in this paper.

Acknowledgments

This work was supported by the National Natural Science Foundation of China (Grant No. 51808209 and 51778222); the Natural Science Foundation of Hunan Province, China (Grant No. 2019JJ50065); the Key Research Project of Hunan Province (Grant 2017SK2224); and the Fundamental Research Funds for the Central Universities through the Project of Young Teacher Growth of Hunan University (Grant No. 531118010081).

References

[1] Connor RJ. Manual for design, construction, and maintenance of orthotropic steel deck bridges. Report No. FHWA-IF-12-027. United States: Federal Highway Administration; 2012.
[2] Troitsky MS. Orthotropic bridges-theory and design. 2nd ed. Cleveland: James F. Lincoln Arc Welding Foundation; 1987.
[3] Tong G, Aiqun L, Jianhui L. Fatigue life prediction of welded joints in orthotropic steel decks considering temperature effect and increasing traffic flow. Struct Health Monit 2008;7(3):189–202.
[4] De Jong FBP, and Boersma PD. Lifetime calculations for orthotropic steel bridge decks. In: The 10th international conference and exhibition-structural faults and repair conference. London; 2003.
[5] Kolstein MH. Fatigue classification of welded joints in orthotropic steel bridge decks [Ph.D thesis]. The Netherlands: Delft University of Technology; 2007.
[6] Wang CS, Zhang Q, Zhang T, Feng YC. Floor-beam web cutout shape analysis to improve the fatigue resistance in orthotropic steel bridge decks. Key Eng Mater 2010;452–453:161–4.
[7] De Backer H, Outtier A, Van Bogaert P. Alternatives for bridge surfacings with orthotropic plated deck: a fatigue point of view. Found Civil Environ Eng 2008;11: 5–16.
[8] Shao XD, Yi DT, Huang ZY, Zhao H, Chen B, Liu ML. Basic performance of the composite deck system composed of orthotropic steel deck and ultrathin RPC layer. J Bridge Eng 2013;18(5):417–28.
[9] Abdelbaset H, Cheng B, Tian L, Li HT, Zhang QH. Reduce hot spot stresses in welded connections of orthotropic steel bridge decks by using UHPC layer: experimental and numerical investigation. Eng Struct 2020;220:110988.
[10] Yuan Y, Wu C, Jiang X. Experimental study on the fatigue behavior of the orthotropic steel deck rehabilitated by UHPC overlay. J Constr Steel Res 2019;157 (JUN.):1–9.
[11] Ding N, Shao XD. Study on fatigue performance of light-weighted composite bridge deck. China Civ. Eng. J 2015;48(1):74–81.
[12] Shao X, Cao J. Fatigue assessment of steel-UHPC lightweight composite deck based on multiscale FE analysis: Case study. J Bridge Eng 2017;23(1):05017015.
[13] Zhang S, Shao X, Cao J, Cui J, Hu J, Deng L. Fatigue performance of a lightweight composite bridge deck with open ribs. J Bridge Eng 2016;21(7):04016039.
[14] Liu Y, Zhang Q, Meng W, Bao Y, Bu Y. Transverse fatigue behaviour of steel-UHPC composite deck with large-size U-ribs. Eng Struct 2019;180(FEB.1):388–99.
[15] Zhu Z, Yuan T, Xiang Z, Huang Y, Zhou YE, Shao X. Behavior and fatigue performance of details in an orthotropic steel bridge with UHPC-deck plate composite system under in-service traffic flows. J Bridge Eng 2018;23(3): 04017142.
[16] Zhang W, Cai CS. Fatigue reliability assessment for existing bridges considering vehicle speed and road surface conditions. J Bridge Eng 2012;17(3):443–53.

[17] Hammouda MMI, Osman HG, Sallam HEM. Mode I notch fatigue crack growth behaviour under constant amplitude loading and due to the application of a single tensile overload. Int J Fatigue 2004;26(2):183–92.
[18] Hammouda, Sherbini, Sallam. Deformation behaviour at the tip of a physically short fatigue crack due to a single overload. Fatigue Fract Eng Mater Struct 1999;22(2):145–51.
[19] AASHTO. AASHTO LRFD bridge design specifications, 6th ed. Washington, D.C.: AASHTO; 2017.
[20] Tong LW, Shen ZY. Fatigue assessment of orthotropic steel bridge decks. China Civil Eng J 2000;33(3):16–21.
[21] Wang Y, Li ZX, Li AQ. Combined use of SHMS and finite element strain data for assessing the fatigue reliability index of girder components in long-span cable-stayed bridge. Theor Appl Fract Mech 2010;54(2):127–36.
[22] Hobbacher A. Recommendations for fatigue design of welded joints and components. New York: Welding Research Council; 2009.
[23] Liu J, Xue H, Chen F. Fatigue assessment of an oil tanker based on common structural rules and the influence of mesh size. J. Shanghai Jiaotong Univ 2008;06:910–3.
[24] Cui C, Zhang Q, Hao H, Li J, Bu Y. Influence of asphalt pavement conditions on fatigue damage of orthotropic steel decks: parametric analysis. J Bridge Eng 2018;23(12):04018093.
[25] Cao JH, Shao XD, Deng L, Gan YD. Static and fatigue behavior of short-headed studs embedded in a thin ultrahigh-performance concrete layer. J Bridge Eng 2017;22(5).
[26] Wang TL, Liu C. Influence of heavy trucks on highway bridges. Report No. FL/DOT/RMC/6672-379. California: Stanford; 2000.
[27] Deng L, Cai CS. Identification of parameters of vehicles moving on bridges. Eng Struct 2009;31(10):2474–85.
[28] Deng L, Cai CS. Development of dynamic impact factor for performance evaluation of existing multi-girder concrete bridges. Eng Struct 2010;32(1):21–31.
[29] Deng L, Cai CS. Identification of dynamic vehicular axle loads: Demonstration by a field study. J Vib Control 2011;17(2):183–95.
[30] Deng L, Cai CS. Bridge model updating using response surface method and genetic algorithm. J Bridge Eng 2010;15(5):553–64.
[31] Shi X, Cai CS, Chen S. Vehicle induced dynamic behavior of short-span slab bridges considering effect of approach slab condition. J Bridge Eng 2008;13(1):83–92.
[32] Dodds CJ, Robson JD. The description of road surface roughness. J Sound Vib 1973;31(2):175–83.
[33] Huang D, Wang TL, Shahawy M. Impact analysis of continuous multigirder bridges due to moving vehicles. J Struct Eng 1992;118(12):3427–43.
[34] Huang D, Wang TL. Impact analysis of cable-stayed bridges. Comput Struct 1992;43(5):897–908.
[35] ISO. Mechanical vibration–road surface profiles–reporting of measured data. Geneva: ISO 8068: (E); 1995.
[36] Li M, Hashimoto K, Sugiura K. Influence of asphalt surfacing on fatigue evaluation of rib-to-deck joints in orthotropic steel bridge decks. J Bridge Eng 2014;19(10):04014038.
[37] Aygül M, Al-Emrani M, Urushadze S. Modelling and fatigue life assessment of orthotropic bridge deck details using FEM. Int J Fatigue 2012;40:129–42.
[38] Cui C, Zhang Q, Luo Y, Hao H, Li J. Fatigue reliability evaluation of deck-to-rib welded joints in OSD considering stochastic traffic load and welding residual stress. Int J Fatigue 2018;111:151–60.
[39] Liu C, Huang D, Wang T. Analytical dynamic impact study based on correlated road roughness. Comput Struct 2002;80(20–21):1639–50.
[40] Miner MA. Cumulative damage in fatigue. J Appl Mech 1945;12(3):A159–64.
[41] Kwon K, Frangopol DM. Bridge fatigue reliability assessment using probability density functions of equivalent stress range based on field monitoring data. Int J Fatigue 2010;32(8):1221–32.
[42] Liu M, Frangopol DM, Kwon K. Fatigue reliability assessment of retrofitted steel bridges integrating monitored data. Struct Saf 2010;32(1):77–89.
[43] Wang W, Deng L, Shao X. Number of stress cycles for fatigue design of simply-supported steel I-girder bridges considering the dynamic effect of vehicle loading. Eng Struct 2016;110:70–8.
[44] De Jong FBP. Overview fatigue phenomenon in orthotropic bridge decks in the Netherlands. 2004 Orthotropic bridge conference. Sacramento; 2004.
[45] Brady SP, O`Brien EJ. Effect of vehicle velocity on the dynamic amplification of two vehicles crossing a simply supported bridge. J Bridge Eng 2006;11(2):250–6.
[46] Wang W, Deng L, Shao X. Fatigue design of steel bridges considering the effect of dynamic vehicle loading and overloaded trucks. J Bridge Eng 2016;21(9):04016048.
[47] Deng L, Yu Y, Zou Q, Cai CS. State-of-the-art review of dynamic impact factors of highway bridges. J Bridge Eng 2014;20(5):04014080.
[48] Nyman WE, Moses F. Calibration of bridge fatigue design model. J Struct Eng 1985;111(6):1251–66.
[49] AASHTO. The manual for bridge evaluation. 3rd ed. Washington, D.C.: AASHTO; 2018.
[50] Lukačević I, Androić B, Dujmović D. Assessment of reliable fatigue life of orthotropic steel deck. Open Eng 2011;1(3):306–15.
[51] Fricke W. Recommended hot-spot analysis procedure for structural details of ships and FPSOs based on round-robin FE analyses. Int J Offshore Polar Eng 2002;12(01):40–8.
[52] Wirsching PH. Fatigue reliability for offshore structures. J Struct Eng 1984;110(10):2340–56.